Accurate Molecular Weight Distribution of Polymers Using Thermal Field-Flow Fractionation with Deconvolution to Remove System Dispersion

MARTIN E. SCHIMPF, P. STEPHEN WILLIAMS, and J. CALVIN GIDDINGS, *Department of Chemistry, University of Utah, Salt Lake City, Utah 84112*

Synopsis

Thermal field-flow fractionation (ThFFF) is an elution process that separates polymeric materials by molecular weight. Elution profiles thus provide approximations to the molecular weight distributions of polymers. The accuracy of such approximate distributions is expected to be improved by accounting for the effect on the elution profile of band-broadening processes in the FFF system. Fortunately this intrinsic band broadening, referred to as system dispersion, is theoretically well-defined in ThFFF. In this article we present an algorithm that corrects ThFFF elution profiles by removing system dispersion. The program is applied to ThFFF fractograms of standard polymers having both narrow and broad molecular weight distributions. The increased accuracy obtained by accounting for system dispersion is demonstrated. For the narrow standard, deconvolution shows that the polydispersity (weight/number-average mol. wt.) is only 1.004. For the broad standard, NBS 706, the molecular weight distribution and parameters obtained agree well with previously published results. Application to a simulated fractogram resulting from mixing five narrow standards helps define the conditions under which accurate molecular weight information can be recovered.

INTRODUCTION

Thermal FFF (ThFFF) is a relatively new methodology applicable to the separation of polymers in solution.[1-4] In ThFFF, as in size-exclusion chromatography (SEC), separation originates in the differential migration of polymer components along the flow axis of an elongated channel. The polymer sample, injected as a plug containing a mixture of polymer components, tends to divide into different volume elements in the channel containing components of equivalent diffusion coefficients.[3] Since diffusion coefficients depend on molecular weight, this fractionation is molecular weight-selective. Thus components of different molecular weight in a polymer sample migrate along the axis of the channel at different average velocities. In ThFFF the resulting retention volume V_r (the volume of carrier liquid required to elute a sample component) for each molecular weight is equal to or greater than the void volume of the channel. In SEC, by contrast, the retention volume is equal to or less than the void volume.

Due, however, to the stochastic nature of migration, with each molecule following a unique random path through the channel, there exists for both ThFFF and SEC a range of statistically possible mean migration velocities for

Journal of Applied Polymer Science, Vol. 37, 2059–2076 (1989)
 CCC 0021-8995/89/072059-18$04.00

each molecular weight. Consequently, a range of elution volumes is found centered around the average value V_r for a given molecular weight component. Hence even a monodisperse polymer zone undergoes dispersion during its migration through a column system.

The dispersion of a polydisperse polymer results from both the differential migration of different molecular weight components and the statistical variation of migration rates among equivalent molecular weight components. The magnitude of the former (selective) dispersion process is characterized by observing the differences in the retention volumes of polymer standards of known molecular weight. It has been found that this "desirable" form of dispersion (desirable because it represents the fractionation of components) is relatively large in ThFFF systems, considerably larger than in SEC systems, as reflected in the higher selectivity of ThFFF.[5] Acting alone, this selective dispersion would generate a fractogram in which the detector signal is represented by $W(V_r)$.

The second dispersion process, system dispersion, can in theory be characterized using monodisperse polymer standards; in practice the polydispersity of even the narrowest standards interferes with the measurement.[1] Alternatively, system dispersion can be determined theoretically because for ThFFF, unlike SEC, an accurate model of system dispersion has been developed.

System dispersion has the effect of contributing additional zone broadening to the "ideal" elution profile $W(V_r)$, where "ideal" refers to the elution profile that would be obtained if all spreading in the channel were molecular weight-selective, directly reflecting the molecular weight distribution. To obtain the ideal elution profile, which leads directly to an accurate molecular weight distribution (MWD), it is necessary to remove the broadening effects of system dispersion from the observed elution profile. Since system dispersion in ThFFF can be modeled relatively rigorously, accurate MWDs should, in theory, be obtainable.

In a previous work[1] we demonstrated the accuracy of system dispersion theory for ThFFF and used the theory to estimate the polydispersities of ultranarrow polymer fractions with an uncertainty of only ± 0.002 polydispersity ($\overline{M}_w/\overline{M}_n$) units. Unfortunately, the method cannot be used to obtain detailed MWDs (as is often desired) for polydisperse samples. The approach used here is intended to remedy this shortcoming and provide accurate distributions for such samples.

In this work we model the superposition of column dispersion on the ideal elution profile by the convolution integral[6]

$$F(V) = \int_0^\infty G(V, V_r) \cdot W(V_r)\, dV_r \tag{1}$$

or, in shorthand form

$$F = G \otimes W \tag{2}$$

where V is the volume of carrier fluid eluted through the channel. Here $W(V_r)$ is the object function representing, as noted, the ideal elution profile, $G(V, V_r)$ is the function representing system dispersion, and $F(V)$ is the image function

or observed elution profile (fractogram). The mathematical technique of removing the effects of $G(V, V_r)$ from $F(V)$ to obtain $W(V_r)$ is termed deconvolution.

If the system dispersion is significant and not accounted for, it will distort the MWD obtained from a fractogram. Recent studies have shown that system dispersion in ThFFF is dominated by nonequilibrium processes, provided solute relaxation by the stop-flow technique is utilized.[1] Although system dispersion causes negligible distortion in the analysis of broad molecular weight distributions (polydispersity $\mu > 1.1$) when low flowrates and high field strengths are used, the fractogram becomes more distorted relative to the ideal elution profile as the flowrate is increased to obtain shorter analysis times.

In this article we describe a deconvolution algorithm for estimating the ideal elution profile by adjusting the ThFFF fractogram to remove the effects of nonequilibrium system dispersion. The removal of nonequilibrium effects allows for the use of faster flowrates without losing accuracy in the resulting MWD.

THEORY

Theoretical and experimental aspects of ThFFF are discussed in several reports.[2-4] The theory essential for the present work is summarized below.

In ThFFF, a thermal gradient is applied across the thin dimension of a narrow ribbonlike channel. The gradient forces the polymer toward the cold (accumulation) wall of the channel by virtue of the phenomenon of thermal diffusion. The resulting buildup of concentration is opposed by ordinary diffusion away from the cold wall. A thin exponential steady-state distribution is soon formed at the wall. Different levels of thermal and ordinary diffusion for different components causes these distributions or "layers" to assume different thicknesses. The distance ℓ from the cold wall to the center of gravity of a particle's distribution is related to the transport coefficients of the polymer–solvent pair under consideration by[2,4]

$$1/\ell = (D_T/D)\, dT/dx \tag{3}$$

where D_T and D are the thermal and ordinary diffusion coefficients for the polymer-solvent system, respectively, and dT/dx is the temperature gradient applied across the channel. The thermal diffusion coefficient D_T has been found empirically to be independent of molecular weight in a given polymer–solvent system.[3] Therefore, mean layer thickness ℓ differs for polymers of different molecular weight due to their unequal rates of ordinary diffusion.

For the further development of the theory, parameter ℓ is generally expressed in the dimensionless form $\lambda = \ell/w$, where λ is termed the retention parameter. The term w is the channel thickness.

Retention

After the component distributions have established their steady-state configurations, flow is initiated in the channel. However, because of the approxi-

mately parabolic flow profile existing across the thin dimension of the channel (in which a higher flow velocity is found in the channel center than near the cold wall), components that form the most compact layers against the wall are carried more slowly down the channel than those forming relatively diffuse layers. The volume V_r of carrier liquid required to elute a component cloud with parabolic flow is related to its dimensionless mean layer thickness λ by[2]

$$R = V^0/V_r = 6\lambda[\coth(1/2\lambda) - 2\lambda] \tag{4}$$

where R is the retention ratio and V^0 is the channel void volume. This equation shows that individual components differing in molecular weight elute with different retention volumes as a result of variations in their characteristics ℓ and λ values, which originate in variations in D. By empirically determining the constants entering the relationship between D and molecular weight for a given polymer–solvent system, ThFFF becomes a high-resolution tool for determining unknown molecular weights and MWDs of polymer samples.

Equation (4) assumes that the carrier liquid has a parabolic velocity profile across the channel thickness. For accurate work this equation must be corrected to account for the departure from parabolic flow induced by the temperature gradient and the attendant changes in the carrier viscosity across the channel thickness. The procedure for obtaining the corrected velocity profile is lengthy and has been discussed elsewhere.[4] The resulting expression is

$$\frac{v(x)}{\langle v(x)\rangle} = \frac{\sum_{i=1}^{5} h_i(x/w)^i}{\sum_{i=1}^{5} \frac{h_i}{(i+1)}} \tag{5}$$

where $v(x)$ is the local velocity at distance x from the cold wall and $\langle v(x)\rangle$ is the cross-sectional average velocity. The parameters h_i are defined as

$$h_1 = \theta b_0 \tag{6a}$$

$$h_2 = (b_0 + \theta b_1)/2 \tag{6b}$$

$$h_3 = (b_1 + \theta b_2)/3 \tag{6c}$$

$$h_4 = (b_2 + \theta b_3)/4 \tag{6d}$$

$$h_5 = b_3/5 \tag{6e}$$

where

$$\theta = -\left(\frac{b_0}{2} + \frac{b_1}{3} + \frac{b_2}{4} + \frac{b_3}{5}\right)\Big/\left(b_0 + \frac{b_1}{2} + \frac{b_2}{3} + \frac{b_3}{4}\right) \tag{7}$$

The parameters b_i are defined as

$$b_0 = a_0 + a_1 T_c \tag{8a}$$

$$b_1 = a_1 S \tag{8b}$$

$$b_2 = -\frac{1}{2}\frac{1}{\kappa_c}(d\kappa/dT)a_1 S^2 \tag{8c}$$

$$b_3 = \frac{1}{2}\left(\frac{1}{\kappa_c}\frac{d\kappa}{dT}\right)^2 a_1 S^3 \tag{8d}$$

Here T_c is the cold wall temperature, κ_c is the thermal conductivity at the cold wall, $d\kappa/dT$ is the rate of change in thermal conductivity with temperature, and

$$S = \Delta T + \frac{1}{\kappa_c}\frac{d\kappa}{dT}\frac{(\Delta T)^2}{2} \tag{9}$$

where ΔT is the temperature difference between the hot and cold walls. Parameters a_0 and a_1 are the linear least-squares fit parameters describing the dependence of carrier fluidity $1/\eta$ on temperature according to

$$\frac{1}{\eta} = a_0 + a_1 T \tag{10}$$

The reduced velocity profile expressed in Eq. (5) cannot be manipulated to yield R as a function of λ in closed form. A closed expression for R has been derived, however, utilizing a third-degree polynomial expression for the velocity profile with one adjustable parameter, ν[7]

$$\frac{v(x)}{\langle v(x)\rangle} = 6\left[(1+\nu)\left(\frac{x}{w}\right) - (1+3\nu)\left(\frac{x}{w}\right)^2 + 2\nu\left(\frac{x}{w}\right)^3\right] \tag{11}$$

Parameter ν can be used to relate R to λ directly as outlined in ref. 7

$$R = 6\lambda\nu(1 - R_p) + R_p \tag{12}$$

Here R_p is the retention ratio obtained from λ for a parabolic velocity profile as calculated from Eq. (4).

Even for components only moderately retained, the sample cloud will be concentrated close to the cold wall, in which case the migration velocity is governed principally by the first-order coefficient in (x/w). Hence, upon equating the first-order term in Eq. (11) with that of Eq. (5) and rearranging, we get

$$\nu = \frac{h_1}{6\sum_{i=1}^{5}\frac{h_i}{(i+1)}} - 1 \tag{13}$$

Using Eq. (13) for ν and Eq. (4) for R_p, a unique value of λ can be assigned to each value of V_r.

System Dispersion

In well-designed ThFFF systems nonequilibrium effects dominate system dispersion as long as the polymer components are allowed to form their steady-state concentration profiles at the cold wall in the absence of axial flow.[1] Extracolumn band broadening can be kept to negligible proportions by using the minimum possible lengths and diameters of narrow-bore tubing between the channel and the detector cell and injection unit. The contribution to band broadening from longitudinal diffusion is negligible due to the small diffusion coefficients of polymers.

Nonequilibrium system dispersion, expressed in terms of the contribution H_n to plate height, takes the following form[8]

$$H_n = \frac{\chi w^2 \langle v \rangle}{D} \tag{14}$$

where $\langle v \rangle$ is the mean velocity of the carrier liquid and χ is the nonequilibrium parameter with the following dependence on R and λ

$$\chi = \frac{2\lambda^2 F'}{R(1 - e^{-1/\lambda})} \tag{15}$$

Here

$$\begin{aligned} F' = {} & 2A\left[6(1+\nu) - (1/\lambda) - (A/\lambda) + 36\nu\lambda^2 - 6\lambda(1+6\nu)\right. \\ & \left. + 18\lambda e^{-1/\lambda}(1+10\nu\lambda)\right] \\ & + 72\lambda^2\left[(1+\nu)^2 - 10\lambda(1+4\nu+3\nu^2)\right. \\ & \left. + 4\lambda^2(7+69\nu+90\nu^2) - 672\nu\lambda^3(1+3\nu) + 4464\nu^2\lambda^4\right] \\ & - 72\lambda^2 e^{-1/\lambda}\left[7 - 2\nu + \nu^2 + 2\lambda(5 - 68\nu + 15\nu^2)\right. \\ & \left. + 4\lambda^2(7 - 69\nu + 180\nu^2) - 672\nu\lambda^3(1-3\nu) + 4464\nu^2\lambda^4\right] \end{aligned} \tag{16}$$

and

$$A = 12\lambda e^{-1/\lambda}(6\nu\lambda - 1)/(1 - e^{-1/\lambda}) \tag{17}$$

Solving for D by the rearrangement of Eq. (3), approximating dT/dx by $\Delta T/w$, and substituting the resulting D into Eq. (14) yields

$$H_n = \frac{\chi w^2 \langle v \rangle}{\lambda D_T \Delta T} \tag{18}$$

The substitution of Eq. (15) into Eq. (18) yields

$$H_n = \frac{2\lambda F' w^2 \langle v \rangle}{D_T R(1 - e^{-1/\lambda})\,\Delta T} \tag{19}$$

Previous studies[1] confirm that system dispersion in ThFFF is accurately defined by Eqs. (14)–(19). These studies also confirm that system dispersion develops as a Gaussian profile.

The general equation of a normalized Gaussian profile centered at retention volume V_r with variance σ_V^2 is given by

$$G(V, V_r) = \frac{1}{(2\pi\sigma_V^2)^{1/2}} \exp\left(-\frac{1}{2} \frac{(V - V_r)^2}{\sigma_V^2} \right) \tag{20}$$

The variance σ_V^2 of this profile (in volume units squared) can be related to plate height by[9]

$$\sigma_V^2 = \frac{H_n V_r^2}{L} \tag{21}$$

Substituting Eq. (21) into Eq. (20), and using Eq. (19) for H_n and the relations $R = V^0/V_r$ and $L = V^0/bw$, we get

$$G(V, V_r) = \frac{V^0}{2wV_r} \left(\frac{D_T(1 - e^{-1/\lambda})\,\Delta T}{\lambda\pi F' V_r \langle v \rangle bw} \right)^{1/2} \times \exp\left(\frac{-(V - V_r)^2 D_T V^{0^2} (1 - e^{-1/\lambda})\,\Delta T}{4\lambda F' V_r^3 \langle v \rangle bw^3} \right) \tag{22}$$

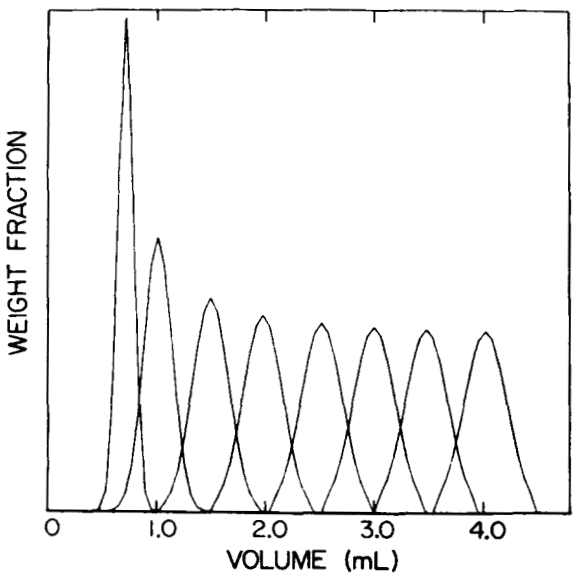

Fig. 1. Theoretical system dispersion profiles as a function of retention volume calculated for polystyrene in ethylbenzene in ThFFF system II (flowrate = 0.8 mL/min, ΔT = 62 K, T_c = 308 K, L_V = 41.9 cm, w = 76 μm, V^0 = 0.66 mL).

where b is the channel breadth. Equation (22) is the explicit volume-based response of the nonequilibrium dispersion function. This is the function that must be deconvoluted from the fractogram to obtain the ideal elution profile $W(V_r)$.

A typical plot of Eq. (22) for polystyrene components in ethylbenzene having different retention volumes is displayed in Figure 1. The curves are normalized so that each contains the same area. The experimental conditions assumed in generating the plots were identical to those used in one of our test cases. Although the effective width (scaled to σ_V) of the individual curves will change with differing experimental conditions, the overall trend in σ_V with retention volume will be unchanged.

METHODS AND PROCEDURES

Deconvolution Algorithm

The deconvolution procedure implemented here was developed by Gold.[10] It is a method of iteration using multiplicative corrections. Ishige et al.[11] used the method to remove the effects of column dispersion from simulated SEC chromatograms. The FFF fractogram, digitized using ™Graphpad, is first smoothed by the method of Savitsky-Golay[12] using a 9-point filter window and a quadratic basis function. Next, the method iteratively estimates W and convolutes the estimate with G to obtain an estimate of F, that is

$$F^{(k)} = G \otimes W^{(k)} \tag{23}$$

where $W^{(k)}$ represents the k-th estimate of the ideal elution profile and $F^{(k)}$ represents the elution profile, or fractogram, predicted for this estimate. In each iteration $W^{(k)}$ is improved by multiplying each digitized point of $W^{(k)}$ by the ratio of the corresponding value of the actual observed elution profile F and the latest estimate of this profile $F^{(k)}$, thereby producing a new estimate for W, that is,

$$W^{(k+1)} = W^{(k)} \cdot \frac{F}{F^{(k)}} \tag{24}$$

The iteration may be given in a single equation

$$W^{(k+1)} = W^{(k)} \cdot \frac{F}{G \otimes W^{(k)}} \tag{25}$$

The first estimate of the ideal elution profile $W^{(1)}$ is simply the observed profile F. Our criterion for stopping the iteration process utilizes a comparison of the polydispersity ($\mu = \overline{M}_w/\overline{M}_n$) calculated from the latest estimate of W with that from the previous estimate. If the relative change is less than 0.01%, then the iteration process is halted. (We will show later that more iterations are sometimes desirable.) The computer code for the entire program is written in Pascal for implementation by the IBM-XT personal computer.

It is necessary to determine λ in Eq. (22) for each discrete point of the digitized elution profile in order to determine the band spreading at that

point. This is accomplished using the Newton-Raphson iterative method to solve for λ consistent with Eq. (12).

Finally, the deconvolution algorithm requires knowledge of the solvent's thermal conductivity and fluidity and their temperature dependence, as well as the thermal diffusion coefficient of the polymer–solvent system. An extensive compilation of viscosity-temperature data can be found in ref. 13. Although thermal conductivity data are less abundant, ref. 14 contains data for a large number of liquids. Thermal diffusion coefficients, shown to be independent of polymer size and shape in a given solvent,[3] can be calculated from retention data using Eq. (3) provided the appropriate diffusion coefficients are known. Values of thermal diffusion coefficients for a number of polymer–solvent systems have been compiled using ThFFF and will be published in the near future. A thermal diffusion coefficient of 9.23×10^{-8} cm^2 s^{-1} K^{-1} was assumed for the polystyrene/ethylbenzene systems under study here.

Molecular Weight Averages and Distributions

For a detector such as that used in this study (and most others), the height of the signal above baseline, s, is linearly related to the mass fraction w of polymer in the eluting stream. With a response of this type, the number-average molecular weight $\overline{M}_n$ of a polymer distribution is obtainable as[15]

$$\overline{M}_n = \frac{\sum s_i}{\sum s_i/M_i} \tag{26}$$

where the summation extends over small equal elements of elution volume (or time) from the beginning to the end of the polymer distribution. The weight-average molecular weight $\overline{M}_w$ is similarly found to be

$$\overline{M}_w = \frac{\sum s_i M_i}{\sum s_i} \tag{27}$$

Polydispersity μ, defined as the ratio $\overline{M}_w/\overline{M}_n$, thus becomes

$$\mu = \frac{\left(\sum s_i M_i\right)\left(\sum s_i/M_i\right)}{\left(\sum s_i\right)^2} \tag{28}$$

In practice, the small volume elements are replaced by digitized increments along the fractogram. Parameter M_i in Eqs. (26)–(28) is calculated from the retention volume V_r at the i-th point of the digitized fractogram using calibration equations established empirically. These equations take the following general form

$$\ln M = c_0 + c_1 \ln\left(V_r - V^0\right) \tag{29}$$

where c_0 and c_1 are constants. For strongly retained components the coefficient c_1 is equal to the reciprocal of system selectivity. The form of the expression allows for the approach to unit retention ratio for components of

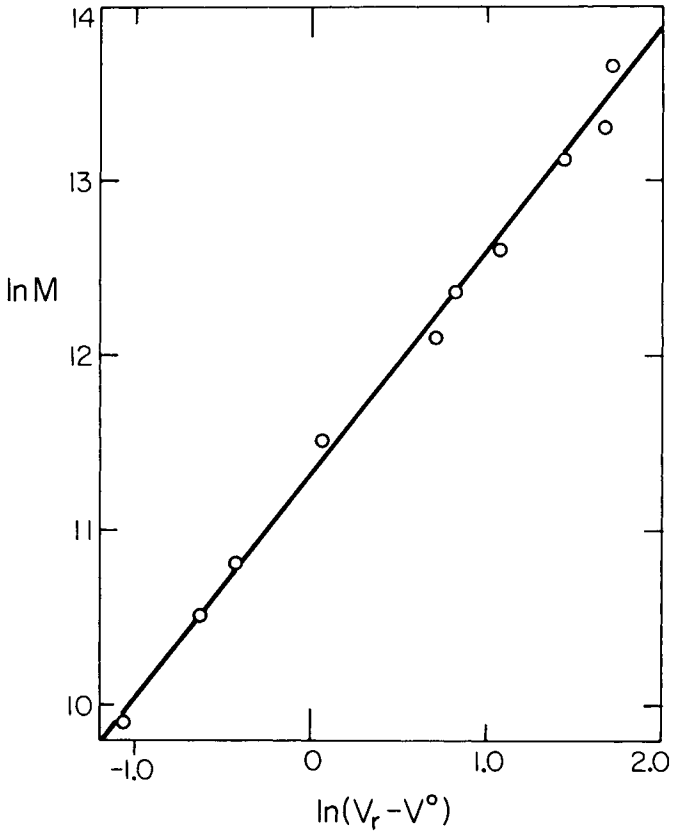

Fig. 2. Calibration plot of molecular weight M versus retention volume V_r for polystyrene in ethylbenzene in system II (ΔT = 62 K, T_c = 308 K, L_V = 41.9 cm, w = 76 μm, V^0 = 0.66 mL).

very low molecular weight. The use of such a calibration equation compensates for any uncertainties in system parameters such as channel thickness. A plot of the calibration expression applicable to polystyrene is ethylbenzene at ΔT = 62°C (T_c = 308°C) is illustrated in Figure 2.

The ideal ThFFF elution profile, $W(V_r)$, is effectively a plot of the polymer concentration c (mass/volume) in the eluting stream versus V_r. In order to obtain a mass-based molecular weight distribution, $m(M)$, we need to transform this profile using the following equation[16]

$$m(M) = c(V_r)\frac{dV_r(M)}{dM} \tag{30}$$

The normalized and digitized form of this equation is

$$m_i = \frac{s_i}{\sum s_i}\frac{\Delta V_r}{\Delta M_i} \tag{31}$$

where ΔV_r is the fixed elution volume element corresponding to one digitized interval.

Instrumentation

Two different ThFFF systems were used to test the deconvolution algorithm. The ThFFF system used to produce the fractogram of the nominal $\overline{M}_w$ = 200,000 ultranarrow polystyrene standard (Pressure Chemical Co., lot 1C) will be referred to as system I and has been described elsewhere.[1] The channel of this system is 76 μm (0.0030 in.) thick, 2.3 cm in breadth, and has a volume-based length L of 31.6 cm. The total void volume is 0.56 mL. A gravity pump was used to avoid pulsing. Peak detection was achieved with a Waters Associates R401 refractive index monitor.

The thermal FFF system used to generate the fractogram of the broad polystyrene standard (NBS 706) has twice the heating power of system I and therefore has the capability of producing a higher ΔT value. This system, referred to as system II, also differs somewhat in the dimensions of the channel, which is 76 μm thick, 2.1 cm in breadth, and has a volume-based length of 41.9 cm. The total void volume of this system is 0.66 mL. The detector is identical to that used in system I while the pump consists of a coil of 1.27 cm (1/2 in.) stainless steel tubing capable of holding approximately one liter of carrier liquid, which is delivered to the ThFFF channel under nitrogen pressure to enable faster flowrates than are achievable with the gravity pump. The carrier liquid used in all cases was ethylbenzene.

RESULTS AND DISCUSSION

In our first application we applied the algorithm to an ultranarrow polystyrene standard obtained from Pressure Chemical Co. (lot 1C). Although the deconvolution algorithm is more appropriately used on broad MWDs, the narrow MWD provides an excellent test of the precision of the algorithm. The fractogram, obtained with System I using a flowrate of 0.14 mL/min, is displayed in Figure 3 along with the calculated ideal elution profile. The sample rate used in digitizing this fractogram was 6 s (0.014 mL) per point. The total number of points in the digitized fractogram is 116, covering the time span from injection to 11.6 minutes. The number of iterations required was 14, with each iteration taking 2 seconds. The total computer time required was less than one minute after the input of the necessary parameters.

In this application, the algorithm lowers the calculated polydispersity μ from 1.02 to 1.004. The calculated weight-average molecular weight $\overline{M}_w$ is 180,000. These values are consistent with those determined by a more time-consuming method used earlier in our laboratory.[1] The manufacturer reports $\overline{M}_w$ = 200,000 and, regarding polydispersity, only that $\mu < 1.06$, a limit far removed from our determination of $\mu = 1.004$.

To examine how well the algorithm can disengage peaks that have been partially or completely merged by column dispersion, we simulated a fractogram (Fig. 4) containing five different molecular weight components. The $\overline{M}_w$ values of the components are 211,600, 263,300, 370,400, 489,500, and 579,200; the polydispersity of each component is 1.005. The input parameters used in the algorithm correspond with the use of system I with a flowrate of 0.4 mL/min and ethylbenzene as the carrier liquid. The ΔT value simulated was 47°C with T_c = 298 K. The sample rate used was 4 s (0.0267 mL) per point covering an elution volume range of 4.37 mL for a total of 165 digitized

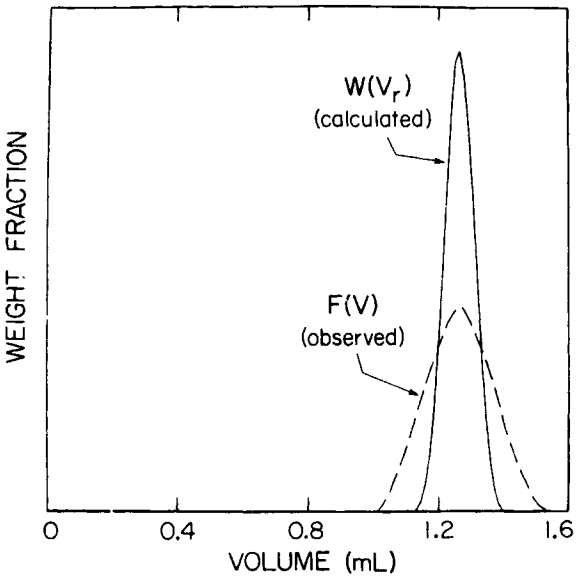

Fig. 3. Fractogram $F(V)$ (---) and calculated ideal elution profile $W(V_r)$ (——) for ultra-narrow polystyrene standard of nominal molecular weight 200,000 (Pressure Chemical lot 1C) using system I (flowrate = 0.14 mL/min, ΔT = 30 K, T_c = 294 K) and stopping criterion as explained in text. Final calculated polydispersity: μ = 1.004.

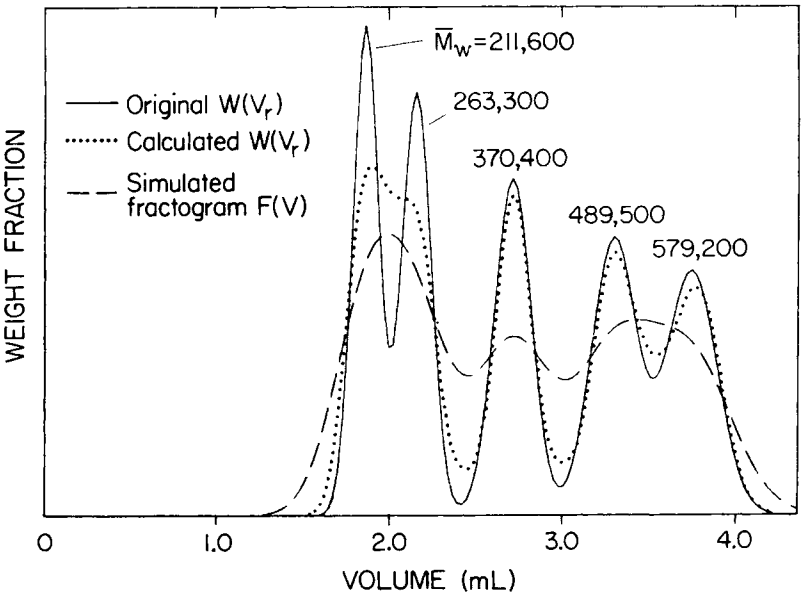

Fig. 4. Simulated ideal elution profile [shown as original $W(V_r)$] (——), simulated fractogram $F(V)$ (---), and calculated $W(V_r)$ (· · · ·) using the stopping criterion explained in text (15 iterations required) for a polystyrene mixture containing five molecular weight components having $\overline{M}_w$ = 211,600, 263,300, 370,400, 489,500, and 579,200, with μ = 1.005 for each component. Conditions simulated are those for ThFFF system I with ethylbenzene as the carrier liquid, flowrate = 0.4 mL/min, ΔT = 47 K, and T_c = 298 K.

points. In the original simulated ideal elution profile $W(V_r)$ the component having nominal $\bar{M}_w$ = 370,400 is nearly baseline resolved from adjacent components. The first component pair, consisting of molecular weights 211,600 and 263,300, are only partially resolved in the original $W(V_r)$, as is the last pair, consisting of molecular weights 489,500 and 579,200. Since system dispersion is not present here, the overlap is due entirely to the intermingling of molecular weights resulting from finite polydispersity. The "observed" elution profile $F(V)$, generated by convoluting this original $W(V_r)$ with the dispersion function G, contains only three peaks, the partially resolved component pairs in the ideal elution profile having completely merged due to column dispersion.

The results of the deconvolution algorithm applied to this simulated fractogram are compared to the original ideal elution profiles in Figures 4 and 5. Figure 4 displays the result when the iteration process is halted after the polydispersity change between iterations is less than 0.01%. In this case the second overlapping pair is resolved by the algorithm and the calculated $W(V_r)$ profile compares well with the original $W(V_r)$. However, the resolution of the first overlapping pair is considerably worse than that of the original $W(V_r)$. The number of iterations performed in this case was 15, each taking 12 s for a total computing time of less than 4 min. If the number of iterations is increased to 50, the resolution of the first pair increases considerably, as displayed in Figure 5. When the number of iterations is increased to 100 the resolution increases further. However, the resolution of the first component pair is still substantially lower than its value in the original $W(V_r)$. The contribution of nonequilibrium dispersion to overall peak width is relatively greater for the first pair and this may account for the slower convergence.

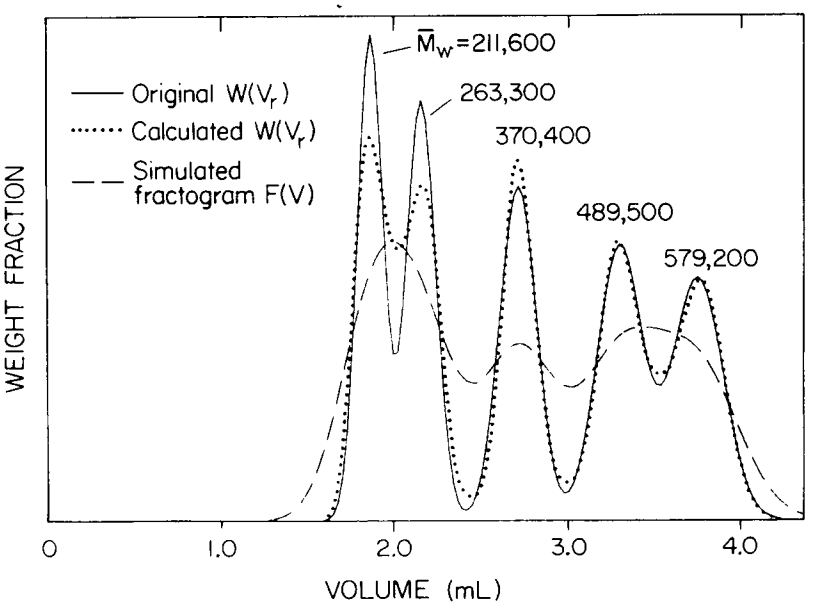

Fig. 5. Simulated (---) and calculated (· · ·) elution profiles obtained under the same conditions as those of Figure 4 except for the use of 50 iterations to get the calculated $W(V_r)$. (——) original $W(V_r)$.

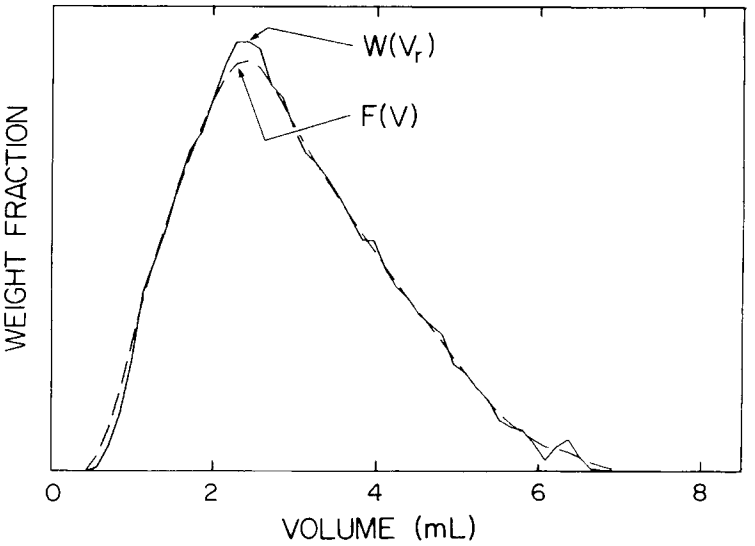

Fig. 6. Observed fractogram $F(V)$ (---) and calculated ideal elution profile $W(V_r)$ (——) for broad polystyrene standard (NBS 706) using system II (flowrate = 0.85 mL/min, ΔT = 62 K, T_c = 308 K) and stopping criterion (12 iterations) as explained in text.

Increasing the sample rate to 3 s (0.02 mL) per point has no apparent effect on these results.

Finally, we tested the algorithm on a broad polystyrene standard (NBS 706) obtained from the National Bureau of Standards. The experimental fractogram $F(V)$, shown in Figure 6, was obtained using a flowrate of 0.85 mL/min in system II. Due to the low molecular weight material in the sample, the main body of the elution profile tends to merge with the void peak. In order to achieve the maximum obtainable resolution of the void peak we utilized the higher heating capability of system II, which allowed for a temperature difference of 62 K (T_c = 308 K) between hot and cold walls.

The sample rate used in digitizing this fractogram was 10 s (0.142 mL) per point. The elution volume range covered was from injection to 7.8 mL. Before applying the deconvolution algorithm, $\overline{M}_w$ and $\overline{M}_n$ are calculated from Eqs. (26) and (27) as 261,500 and 123,200, respectively, giving μ = 2.12. The reported values are $\overline{M}_w$ = 258,000, obtained from low angle light scattering, and $\overline{M}_n$ = 137,500, obtained from membrane osmometry, giving μ = 1.88. In applying the deconvolution algorithm we notice that oscillations appear early in the iteration process. The ideal elution profile $W(V_r)$ displayed in Figure 6 is obtained using the previously mentioned stopping criteria, requiring 12 iterations at 1.9 s per iteration. Before applying the deconvolution algorithm the void peak was removed, as indicated by its absence in both the observed fractogram $F(V)$ and the ideal elution profile $W(V_r)$. The values $\overline{M}_w$ and $\overline{M}_n$ calculated from this $W(V_r)$ using Eqs. (26) and (27) are 261,200 and 144,800, respectively, giving μ = 1.80.

If the iteration process is continued the ideal elution profile converges to that displayed in Figure 7 after 50 iterations. Additional iterations result in no further changes in the ideal elution profile. The calculated molecular weight

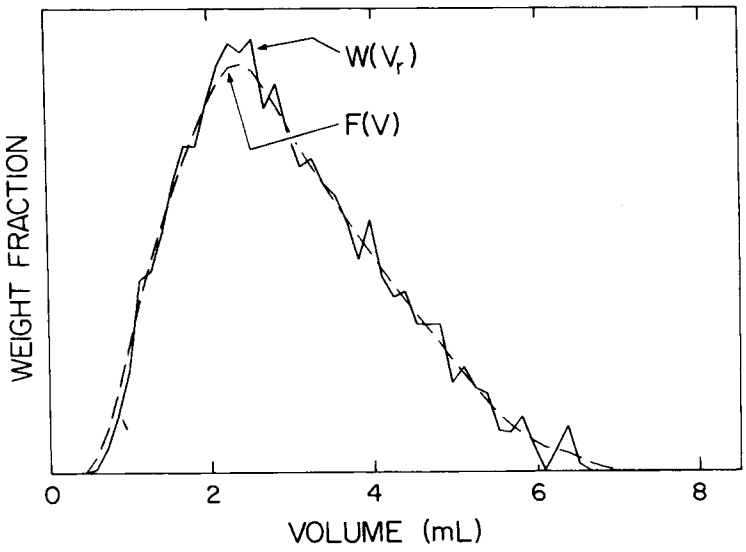

Fig. 7. Fractogram $F(V)$ (---) and calculated $W(V_r)$ (——) for NBS 706 after 50 iterations using system II under same conditions as stated in Figure 6.

averages after 50 iterations are not significantly different from those obtained after 12 iterations: $\overline{M}_w$ = 261,200 and $\overline{M}_n$ = 144,900. The oscillations can be avoided by smoothing the ideal elution profile between iterations. Figure 8 displays the smoothed $W(V_r)$ obtained in this case.

In smoothing the ideal elution profile $W(V_r)$ we are convoluting it with a filtering function. Therefore, additional dispersion is added. This has two consequences. First, the computing time per iteration increases slightly (to

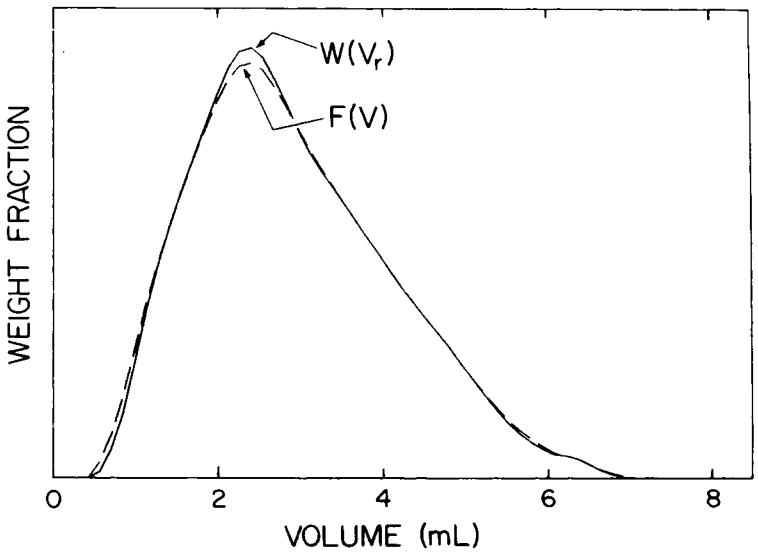

Fig. 8. Fractogram $F(V)$ (---) and calculated $W(V_r)$ (——) for NBS 706 using smoothing procedure and conditions of Figure 6.

2.5 s) but the number of iterations required for convergence is halved (only 6 are required). More importantly, the molecular weight averages can be expected to change with a resulting increase in the calculated polydispersity. In order to minimize such effects, an additional iteration was performed after the stopping criterion was reached without subsequent smoothing. In this case $\overline{M}_w$ and $\overline{M}_n$ are found to be 261,100 and 140,300, resulting in a polydispersity increase from 1.80 to 1.86.

The comparison of Figure 8 with Figure 3 shows clearly that the removal of column dispersion results in a more visible change in the elution profile for the narrow distribution than for the broad distribution. The reason for this, of course, is that the relative contribution of system dispersion to the overall width of the fractogram is much greater for the narrow distribution.

The MWD calculated from the ideal elution profile of Figure 8 using Eq. (31) is illustrated in Figure 9. An MWD obtained by Provder and Rosen[17] using SEC is shown for comparison. There is no clear explanation for the discrepancy.

Molecular weight averages obtained by the various methods are summarized in Table I. It is apparent that $\overline{M}_w$ remains relatively unaffected by smoothing or by the deconvolution procedure in general. The value of $\overline{M}_w$ obtained by ThFFF agrees well with that obtained by light scattering and SEC.

The term $\overline{M}_n$, on the other hand, changes significantly with small changes in the low retention volume region of the ideal elution profile. Although $\overline{M}_n$ values obtained by osmometry contain a significant amount of uncertainty ($\sim$ 10% relative), these values can usually be considered an upper limit to the true value due to diffusion of monomer through the membrane.[18] It is therefore likely that the $\overline{M}_n$ value obtained by ThFFF for this sample is too

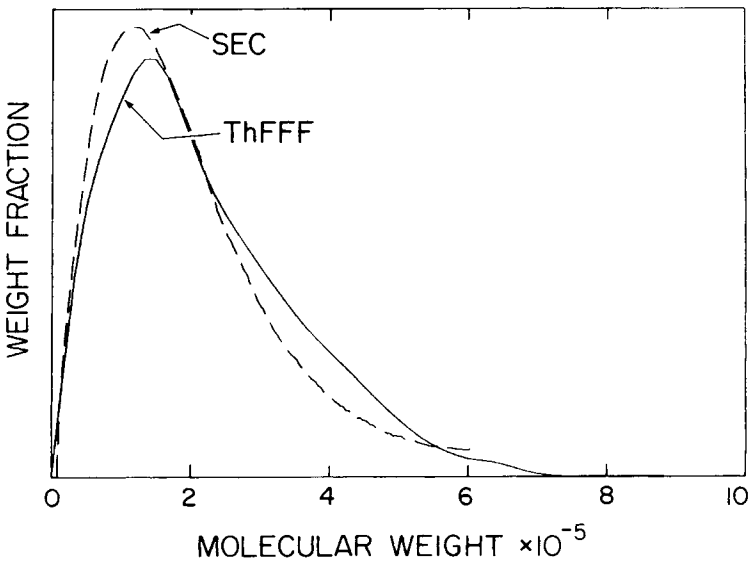

Fig. 9. Molecular weight distribution for polystyrene standard NBS 706 obtained from the $W(V_r)$ profile displayed in Figure 8 (solid line). A distribution obtained by SEC[17] is shown for comparison (broken line).

TABLE I
Summary of Molecular Weight Averages and Polydispersities Obtained for Polystyrene Standard NBS 706 Using Various Methods

	$\overline{M}_w$	$\overline{M}_n$	$\mu = \overline{M}_w/\overline{M}_n$
Reported by supplier	258,000[a]	137,500[b]	1.88
SEC[17]	261,000	135,000	1.93
ThFFF before deconvolution	261,500	123,200	2.12
ThFFF after deconvolution			
no smoothing	261,200	144,800	1.80
with smoothing	261,100	140,300	1.86

[a] Light scattering.
[b] Osmometry.

high. This is not surprising considering the sensitivity of calculated $\overline{M}_n$ values to the low molecular weight end of the MWD and the inability of the present ThFFF system to significantly retain components of low molecular weight. The use of higher ΔT values will undoubtedly improve this situation. While system II is limited to $\Delta T \simeq 62°C$, values to 150°C have been achieved previously, although in a thicker channel.[19] Efforts to improve instrumentation toward higher ΔT without increasing w are underway in our laboratory.

CONCLUSIONS

An algorithm for removing the effects of column dispersion from ThFFF fractograms has been developed. Application to a narrow polystyrene standard shows a remarkably low polydispersity, $\mu = 1.004$. Application to a simulated fractogram representing a series of narrow molecular weight fractions demonstrates the general ability of the algorithm to resolve molecular weight components that are merged in the fractogram as a result of column dispersion, but with some difficulties for strongly overlapping peaks. Additionally, application to a broad polystyrene standard, NBS 706, shows good agreement with other methods, and provides guidelines on various procedural variations that can be used to meet specific goals. We show that the analysis of broad MWDs is limited by poor retention of low molecular weight components by the ThFFF apparatus, necessitating an improvement in instrumentation toward increasing the maximum achievable temperature drop ΔT.

The high sensitivity of calculated $\overline{M}_n$ to the elution profile at the low molecular weight extreme necessitates a high signal to noise ratio (S/N) if accurate polydispersities are to be obtained. If S/N were relatively low, the deconvolution process would be of little value because of the poor inherent precision. Without smoothing, the generation of oscillations in the solution could actually worsen the precision of the experimental results.

We note, in conclusion, that one of the most promising aspects of deconvolution is its ability to maintain good MWD accuracy despite moderately increasing levels of band broadening. This should permit the use of much higher speed runs, in which fractogram resolution is lost due to increasing band broadening, without an unacceptable sacrifice in the fidelity of the MWD curve.

This work was supported by Grant No. CHE-8218503 from the National Science Foundation.

References

1. M. E. Schimpf, M. N. Myers, and J. C. Giddings, *J. Appl. Polym. Sci.*, **33**, 117 (1987).
2. J. C. Giddings, *Sep. Sci. Technol.*, **19**, 831 (1984).
3. M. E. Schimpf and J. C. Giddings, *Macromolecules*, **20**, 1561 (1987).
4. J. J. Gunderson, K. D. Caldwell, and J. C. Giddings, *Sep. Sci. Technol.*, **19**, 667 (1984).
5. J. J. Gunderson and J. C. Giddings, *Anal. Chim. Acta*, **189**, 1 (1986).
6. P. A. Jansson, *Deconvolution with Applications in Spectroscopy*, Academic, New York, 1984.
7. M. Martin and J. C. Giddings, *J. Phys. Chem.*, **2**, 147 (1979).
8. J. C. Giddings, Y. H. Yoon, K. D. Caldwell, M. N. Myers, and M. E. Hovingh, *Sep. Sci. Technol.*, **10**, 47 (1975).
9. J. C. Giddings, *Dynamics of Chromatography*, Dekker, New York, 1965.
10. R. Gold, AEC Research and Development Report ANL-6984, Argonne National Laboratory, Argonne, Illinois, 1964.
11. T. Ishige, S. I. Lee, and A. E. Hamielic, *J. Appl. Polym. Sci.*, **15**, 1607 (1971).
12. A. Savitsky and M. J. E. Golay, *Anal. Chem.*, **36**, 1627 (1964).
13. H. H. Landolt, in *Zahlen Werte und Functionen aus Physik, Chemie, Astronomie, Geophysik und Technik*, Springer, Berlin, 1969, Vol. 2, Part 5, Sect. A.
14. D. T. Jamieson and J. S. Tudhope, *The Thermal Conductivity of Liquids: A Survey to 1963*, NEL Report No. 137, 1964.
15. L. H. Tung, in *Polymer Fractionation*, M. J. R. Cantow, Ed., Academic, New York, 1967.
16. J. C. Giddings, M. N. Myers, F. J. F. Yang, and L. K. Smith, *Colloid and Interface Science*, Vol. IV, M. Kerker, Ed., Academic, New York, 1976, pp. 381–398.
17. T. Provder and E. M. Rosen, *Sep. Sci. Technol.*, **5**, 437 (1970).
18. F. W. Billmeyer, Jr., *Textbook of Polymer Science*, 2nd ed., Wiley Interscience, New York, 1971.
19. J. C. Giddings, L. K. Smith, and M. N. Myers, *Anal. Chem.*, **47**, 2389 (1975).

Received April 15, 1988
Accepted April 21, 1988